In situ lattice measurement of the bcc phase boundary in Mg on the principal shock Hugoniot

D. Milathianaki, D. C. Swift, J. Hawreliak, B. S. El-Dasher, J. M. McNaney, H. E. Lorenzana, and T. Ditmire

Phys. Rev. B **86**, 014101 — Published 5 July 2012

DOI: 10.1103/PhysRevB.86.014101

In situ Lattice Measurement of the *Bcc* Phase Boundary in Mg on the Principal Shock Hugoniot.

D. Milathianaki,[1] D. C. Swift,[2] J. Hawreliak,[2] B. S. El-Dasher,[2] J. M. McNaney,[2] H. E. Lorenzana,[2] and T. Ditmire[3]

[1] *SLAC National Accelerator Laboratory, Menlo Park, CA 94025, USA*

[2] *Lawrence Livermore National Laboratory, P.O. Box 808, Livermore, California 94551, USA*

[3] *Texas Center for High Intensity Laser Science, Department of Physics, University of Texas, Austin, Texas 78712, USA*

We report on nanosecond resolution lattice measurements of shock-compressed Mg in the *hcp* and *bcc* phases between 12 and 45 GPa. X-ray diffraction signals consistent with a compressed *bcc* lattice were captured above a shock pressure of 26.2±1.3 GPa. Our results are in agreement with the phase boundary calculated by Moriarty and Althoff using the generalized pseudopotential theory in the pressure and temperature region intersected by the principal shock Hugoniot.

PACS numbers: 64.70.K-, 62.50.Ef, 61.05.cp

The critical role of the pressure–induced *s* to *d* band electron transfer on the structural stability and physical properties, such as superconductivity, of metals has been studied extensively over the years [1-4]. High pressure structural sequences in 3rd period metals have also been elucidated when taking into account the lowering and filling under compression of the initially vacant *d*-band [5, 6]. The *hcp* to *bcc* phase transition in Mg is an example of such structural change attributed to a pressure-induced *d*-band population. A number of first principles calculations within the framework of density functional theory [7-10] have attempted to define the *hcp-bcc* phase boundary in Mg taking advantage of its simple atomic arrangement and nearly-free electron properties up to pressures of ~100 GPa [11-14]. However, because of the small free energy difference between the competing crystal structures, the location of the *hcp-bcc* phase boundary has been predicted with a variation of ~5 GPa at room temperature, to >8 GPa for T>500 K.

To date, the sole experimental measurement of the *hcp-bcc* phase boundary in Mg was performed under quasi-static conditions by Olijnyk *et al.* [15] at 300 K and ~50±6 GPa. This uncertainty in the pressure value of the phase boundary has not permitted comparison between different *ab initio hcp-bcc* boundary calculations. Furthermore, diamond anvil cell (DAC) x-ray diffraction measurements by Errandonea *et al.* [16] for P>7.5 GPa and T>1100 K have reported no evidence of a *bcc* phase in Mg.

Shock-loading [17-19] is of particular interest in the study of the *hcp* to *bcc* phase transition in Mg as the desired pressure (and temperature) regime can be easily accessed and characterized with traditional velocimetry techniques [20]. In addition, the shock itself provides a fiducial for measuring time-dependent processes in the lattice, thus yielding important information on the kinetics of the phase transition during dynamic

loading. In general, combined with temporally and spatially resolved lattice measurements provided by nanosecond x-ray diffraction [21], shock-loading can offer new insights into the transient phase transition mechanisms. The significance of nanosecond x-ray diffraction in the investigation of shock-induced phase transitions was recently demonstrated in the measurement of the α–ε transition in single crystal Fe [22].

In this paper, we present a lattice measurement of the *hcp* to *bcc* phase transition in Mg induced by shock-loading. This structural change has never been observed in previous Mg shock experiments employing exclusively Doppler velocimetry (VISAR), since the <1% volume change of the transition is practically undetectable by this technique. Here, *in situ* lattice evidence of the *bcc* phase together with a real-time calibration of the sample pressure allowed determination of the *hcp*-*bcc* phase boundary. Our data indicated that the phase boundary intersects the principal Hugoniot at a shock pressure of 26.2±1.3 GPa. The small uncertainty of our measurements enabled us to differentiate between various calculated phase boundaries, specifically validating one previously published model by Moriarty and Althoff [14] using the generalized pseudopotential theory (GPT). Furthermore, our time-resolved measurement provided an upper time limit of <1 ns for the bulk material to transform into the *bcc* phase. This time scale is consistent with the proposed martensitic mechanism of the *hcp* to *bcc* transition in Mg [23].

The experiment was performed at the JANUS two-beam, kJ-level laser at Lawrence Livermore National Laboratory. A 4.7 keV, 3 ns, point x-ray source was generated by one of the 527 nm laser beams when incident on a 12 μm thick Ti foil [24] with a peak intensity of ~4×10^{14} W/cm^2 (Figure 1). He$_\alpha$-like x-rays emitted over 4π sr

from the thermal plasma were collimated by a series of pinholes to a ~2 mm diameter spot size on the target. The sample and x-ray source were placed on the axis of a 6.9 cm diameter cylindrical detector described in detail elsewhere [25]. The Debye-Scherrer diffraction rings from grains satisfying the Bragg condition $2d_{hkl}\sin\theta=\lambda$ were recorded on imaging plate detectors wrapped around the perimeter of the cylinder. The diffraction signal recorded in this cylindrical arrangement took the form of straight lines at the corresponding Bragg angle 2θ upon unfolding the imaging plates, thus considerably simplifying the data analysis.

Samples of 50 μm thick, 99.98% pure rolled Mg foil coated with a 39 μm parylene-N/80 nm Al ablator layer were used in the experiments. The static texture of the sample was characterized with a continuous Cu K_α laboratory source prior to shock-loading. The texture and orientation of the samples relative to the collimated x-ray source resulted in certain Mg planes appearing exclusively in reflection ($(002)_{hcp}$ and $(102)_{hcp}$), or in transmission ($(100)_{hcp}$), or both ($(101)_{hcp}$). However, texture did not compromise our measurements as the cylindrical diffraction geometry employed was able to record full Debye-Scherrer rings.

Shocks were ablatively driven in the parylene-N coating using single 527 nm laser pulses with peak intensity between $4\text{x}10^{11}$-$1.5\text{x}10^{12}$ W/cm^2 resulting in shock pressures in Mg between 12 and 45 GPa. A trapezoidal laser temporal profile with <100 ps rise time and 6 ns duration was chosen to provide a steady amplitude shock front at the ablator/Mg interface, a behavior confirmed by 1D Lagrangian hydrodynamics simulations [26]. Spatially uniform shock-loading over a 1 mm^2 area was achieved by placing the sample front surface at the focus of a KPP phase plate. Two-channel line-imaging Doppler

velocimetry was implemented to verify the Hugoniot end state pressure and material response via measurement of the sample's rear free surface velocity upon shock breakout.

Single-shot x-ray diffraction signal integrated over the ~3 ns x-ray pulse duration was recorded on the imaging plate detectors in transmission and in reflection from the sample. Diffraction data from the unfolded imaging plate detectors at 12.7±0.5 GPa and 44.5±1.1 GPa are shown in Figure 2. The sample thickness probed corresponded approximately to the attenuation length of the 4.7 keV x-rays incident on Mg at 45º with respect to the sample surface, namely 22 μm. Static reference signal was captured on every shot by timing the x-ray pulse to start ~1 ns before the arrival of the shock front at the ablator/Mg interface. In Figure 2, dashed lines indicate line profiles from static *hcp* diffraction peaks, whereas dash-dotted lines indicate line profiles from compressed *hcp* diffraction peaks.

For shock pressures below 26 GPa, compression of the $(100)_{hcp}$, $(002)_{hcp}$, $(101)_{hcp}$ and $(102)_{hcp}$ planes was evident in the diffraction images as additional peaks parallel to the static reference peaks at a larger diffraction angle 2θ. Lattice compression for the observed (*hkl*) planes was extracted from the shift in 2θ measured between the respective static and compressed Mg diffraction peaks. The difference in 2θ between the static and compressed peaks was measured by fitting Gaussian profiles, using a least squares optimization routine, to the line profiles extracted from the diffraction signal. In the data shown here, the $(100)_{hcp}$ was compressed by 7.3%, the $(002)_{hcp}$ by 6.8%, the $(101)_{hcp}$ by 7.4% and the $(102)_{hcp}$ by 6.8%. Within the uncertainty of our measurement (0.2%), the observed lattice strains along different orientations were approximately equal, thus implying isotropic lattice compression.

For shock pressures above 26 GPa, the number of diffraction peaks from shock-compressed planes decreased, as shown in Figure 2b. Apart from the static reference peaks, only a single diffraction peak was observed from the shocked state in both the transmitted and reflected direction. This peak was interpreted as either a compressed *hcp* or *bcc* phase by comparing the material density in either phase against the Mg shock Hugoniot.

Material density was obtained from the interplanar spacing measured via x-ray diffraction assuming an isotropically compressed end state. This assumption was supported in our diffraction measurements by the absence of significant strength effects that would have been exhibited as a variation in the measured lattice strain along the azimuthal direction. The pressure estimated by velocimetry and the compressed to static density ratio measured by nanosecond x-ray diffraction assuming isotropic compression, $\frac{\rho}{\rho_0} = \left(\frac{d_0}{d}\right)^3 = \left(\frac{\sin\theta}{\sin\theta_0}\right)^3$ is plotted in Figure 3. Below 26 GPa, the data were in good agreement with the Mg shock Hugoniot calculated using an EOS from SESAME table #2860 [27], consistent with our assumption of negligible strength effects. Above 26 GPa, the diffraction angle 2θ measured was assumed to originate from either an *hcp* or *bcc* compressed lattice. Calculation of a density ratio assuming diffraction from compressed $(101)_{hcp}$ planes resulted in a significant deviation from the Mg shock Hugoniot. A similar result was obtained assuming diffraction from compressed $(002)_{hcp}$ planes. In contrast, assignment of a density ratio from compressed $(110)_{bcc}$ planes overlaid our data points the closest to the Mg shock Hugoniot.

Since the expected *hcp-bcc* $\Delta V/V_0$ of <1% corresponds to a lattice distortion with an imperceptible discontinuity in the pressure-volume plot, we deduced that the new diffraction peak observed above a shock pressure of 26 GPa belonged to compressed $(110)_{bcc}$ planes. At 44.5±1.1 GPa the lattice strain in the $(110)_{bcc}$ plane was measured to be 13.1% in transmission and 12.3% in reflection resulting in a material density ratio of 1.52 and 1.49 respectively. Measurement of a compressed *bcc* phase on the principal Hugoniot was determined above P=26.2±1.3 GPa.

In this study, shock loading to end states on the principal Hugoniot provided access to a P-T region in the Mg phase diagram where calculated *bcc* phase boundaries vary significantly. In this way, we were able to assess the performance of different exchange correlation potential approximations, unlike data previously obtained at 300 K where phase boundary predictions by the local density approximation (LDA) and general gradient approximation (GGA) overlap closely. Figure 4 shows the calculated *bcc* phase boundaries in Mg together with the locus of end states that we probed on the principal Hugoniot. The principal Hugoniot intersects the *bcc* GGA boundary at P=32 GPa, T=1270 K, the LDA *bcc* boundary at P= 30 GPa, T=1155K and the LDA-GPT *bcc* boundary at P=27 GPa, T=1020 K. Our lattice measurement of a *bcc* phase above 26 GPa closely agrees with the LDA-GPT approximation [14]. Thus, the lower pressure predicted for the *bcc* phase boundary by the LDA-GPT method is consistent with our experimental observation.

The uniformity of the new line representing the compressed $(110)_{bcc}$ suggests no significant texture in the new phase. This could be attributed to an original *hcp* phase texture that is favorable towards the atomic re-arrangement mechanism, as well as a

highly degenerate transition pathway. The proposed *hcp* to *bcc* transition mechanism in Mg consisting of a shuffling of planes such that the $(001)_{hcp}$ coincides with the $(110)_{bcc}$, has a twelve-fold degeneracy. Furthermore, the intensity of the new $(110)_{bcc}$ relative to the compressed *hcp* lines is in agreement with the DAC diffraction data of Olijnyk and Holzapfel [15] above the transition pressure. Specifically Olijnyk and Holzapfel [15] reported a strong decrease in the intensity of the compressed *hcp* peaks upon appearance of the $(110)_{bcc}$ signal, similar to the our observed diffraction intensity above 26 GPa. In addition, the low scattering intensity observed by Olijnyk and Holzapfel in *bcc* planes other than $(110)_{bcc}$ supports the absence of additional *bcc* diffraction peaks in our experiments due to the limited signal to noise ratio of our technique. A *dhcp* phase observed by Errandonea *et al*. in the low pressure-high temperature region of the Mg phase diagram could not be verified by our measurements; a diffraction geometry with improved angular resolution would be required for the detection of such small structural change from the original *hcp* phase.

In summary, using laser-based nanosecond x-ray diffraction and shock-loading we obtained a direct lattice measurement of the *hcp* to *bcc* phase transition in polycrystalline Mg. The peak shock pressure above which the *bcc* phase became evident was 26.2±1.3 GPa in agreement with the *bcc* phase boundary calculated by Moriarty and Althoff [14] using a total energy pseudopotential method. The subnanosecond timescale of the phase transition implied by the shock-loading conditions was in agreement with the kinetics of a martensitic transformation.

The authors would like to thank Mike Saculla and the JANUS laser facility team, especially Dwight Price, for their support in this study. This work was performed under

the auspices of the U.S. Department of Energy by Lawrence Livermore National Laboratory under Contract DE-AC52-07NA27344. Funding was provided by the LLNL LDRD program, Project PLS-08ERD038.

[1] H. Olijnyk and W. B. Holzapfel, Phys. Lett. A **100**, 191 (1984).

[2] M. Sakata, Y. Nakamoto, K. Shimizu, T. Matsuoka, and Y. Ohishi, Phys. Rev. B **83** (2011).

[3] P. Soderlind, R. Ahuja, O. Eriksson, B. Johansson, and J. M. Wills, Phys. Rev. B **49**, 9365 (1994).

[4] L. Stixrude, Phys. Rev. Lett. **108** (2012).

[5] J. A. Moriarty and A. K. McMahan, Phys. Rev. Lett. **48**, 809 (1982).

[6] A. K. McMahan and J. A. Moriarty, Phys. Rev. B **27**, 3235 (1983).

[7] A. DalCorso, A. Pasquarello, A. Baldereschi, and R. Car, Phys. Rev. B **53**, 1180 (1996).

[8] P. Hohenberg and W. Kohn, Phys. Rev. B **136** (1965).

[9] W. Kohn and L. J. Sham, Phys. Rev. B **140** (1965).

[10] J. A. Moriarty, Phys. Rev. B **16**, 2537 (1977).

[11] G. R. Chavarria, Phys. Lett. A **336**, 210 (2005).

[12] F. Jona and P. M. Marcus, J. Phys.-Condens. Mat. **15**, 7727 (2003).

[13] S. Mehta, G. D. Price, and D. Alfe, J. Chem. Phys. **125**, 7 (2006).

[14] J. A. Moriarty and J. D. Althoff, Phys. Rev. B **51**, 5609 (1995).

[15] H. Olijnyk and W. B. Holzapfel, Phys. Rev. B **31**, 4682 (1985).

[16] D. Errandonea, Y. Meng, D. Hausermann, and T. Uchida, J. Phys.-Condens. Mat. **15**, 1277 (2003).

[17] G. E. Duval and R. A. Graham, Rev. Mod. Phys. **49**, 523 (1977).

[18] A. Benuzzi-Mounaix, et al., Plasma Phys. Contr. F. **48**, B347 (2006).

[19] D. C. Swift, T. E. Tierney, R. A. Kopp, and J. T. Gammel, Phys. Rev. E **69** (2004).

[20] P. M. Celliers, et al., Rev. Sci. Instrum. **75**, 4916 (2004).

[21] J. S. Wark, R. R. Whitlock, A. A. Hauer, J. E. Swain, and P. J. Solone, Phys. Rev. B **40**, 5705 (1989).

[22] D. H. Kalantar, et al., Phys. Rev. Lett. **95** (2005).

[23] R. M. Wentzcovitch, Phys. Rev. B **50**, 10358 (1994).

[24] D. W. Phillion and C. J. Hailey, Phys. Rev. A **34**, 4886 (1986).

[25] J. Hawreliak, H. E. Lorenzana, B. A. Remington, S. Lukezic, and J. S. Wark, Rev. Sci. Instrum. **78** (2007).

[26] D. C. Swift, et al., Phys. Rev. E **78** (2008).

[27] J. D. Johnson and S. P. Lyon, Vol. LA-UR-92-3407, LANL, Los Alamos, 1992.

[28] S. P. Marsh, LASL Shock Hugoniot Data, University of California Press, Berkeley, 1980.

FIG. 1. (not to scale) Experimental geometry for *in situ* x-ray diffraction measurements from shocked polycrystalline samples

FIG. 2. X-ray diffraction data and line profiles captured in transmission and reflection from polycrystalline Mg at 12.7±0.5 and 44.5±1.1 GPa respectively. a) Static and compressed diffraction signal from the $(100)_{hcp}$, $(101)_{hcp}$ $(002)_{hcp}$, and $(102)_{hcp}$ planes at 12.7±0.5 GPa and b) diffraction signal from the compressed $(110)_{bcc}$ plane at 44.5±1.1 GPa. No evidence of the compressed Mg parent phase (*hcp*) at this pressure.

FIG. 3. Plot of shock pressure against the material compressed to static density ratio. The principal Hugoniot from SESAME table #2860 [27] and that measured by Marsh [28] are also shown. Above 26 GPa, a *bcc* interpretation of the data appeared to be consistent with the Mg shock Hugoniot and the small volumetric change of the *hcp* to *bcc* phase transition.

FIG. 4. The calculated P-T phase diagram of Mg from various *ab initio* methods including the experimental points obtained in this study and by Olijnyk and Holzapfel [15]. The *bcc* phase measured above 26 GPa agrees well with the phase boundary calculated from generalized pseudopotential theory.

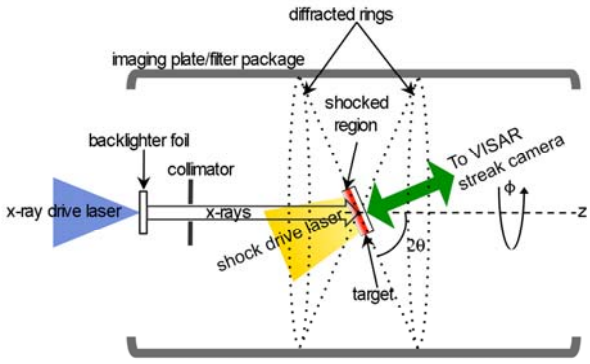
diffracted rings
imaging plate/filter package
shocked
region
backlighter foil
collimator
To VISAR
streak camera
x-ray drive laser
x-rays
shock drive laser
z
2θ
target

FIG. 1.

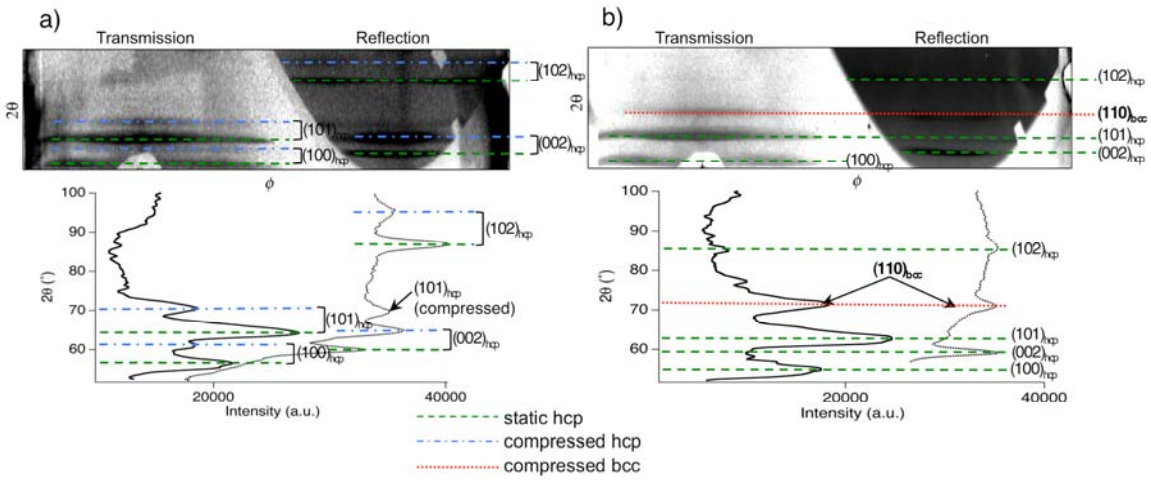

FIG. 2. PLEASE PRINT WITH 2 COLUMN WIDTH

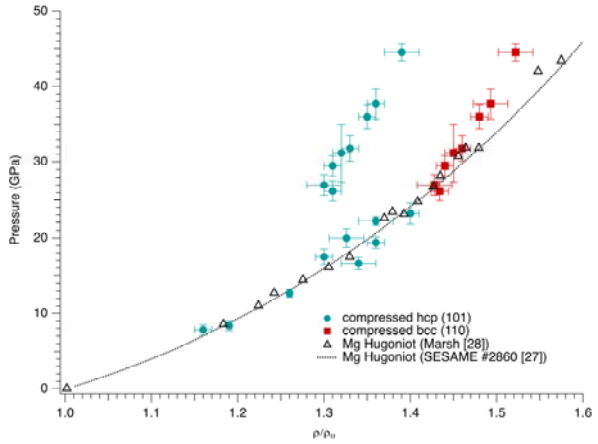
Pressure (GPa)
50
40
30
20
10
0
1.0
1.1
1.2
1.3
1.4
1.5
1.6
ρ/ρ0
compressed hcp (101)
compressed bcc (110)
Mg Hugoniot (Marsh [28])
Mg Hugoniot (SESAME #2860 [27])

FIG. 3.

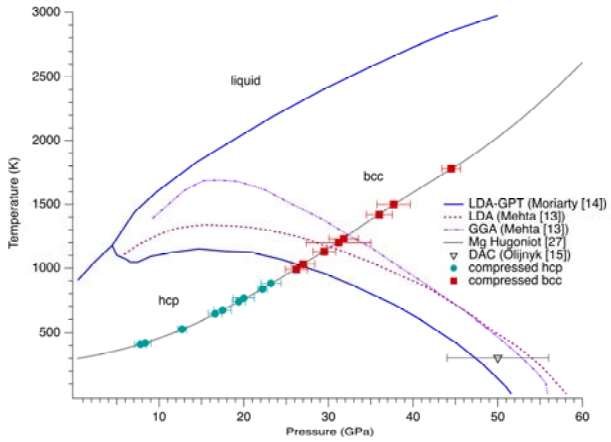
liquid
bcc
hcp
Temperature (K)
Pressure (GPa)
LDA-GPT (Moriarty [14])
LDA (Mehta [13])
GGA (Mehta [13])
Mg Hugoniot [27]
DAC (Olijnyk [15])
compressed hcp
compressed bcc

FIG. 4.